Optics Letters

Attitude metrology based on the field-of-view effect of birefringence using high-speed polarimetry

Song Zhang,[1] Hao Jiang,[1,2] Honggang Gu,[1,3] Xiuguo Chen,[1] and Shiyuan Liu[1]

[1]State Key Laboratory of Digital Manufacturing Equipment and Technology, Huazhong University of Science and Technology, Wuhan 430074, China
[2]e-mail: hjiang@hust.edu.cn
[3]e-mail: honggganggu@hust.edu.cn

Received 7 January 2020; revised 29 February 2020; accepted 1 March 2020; posted 2 March 2020 (Doc. ID 387626); published 31 March 2020

A novel, to the best of our knowledge, optical method using a high-speed polarimetry is proposed for real-time attitude tracking in an ultra-large measurement range. The attitude metrology utilizes the field-of-view effect in birefringent crystals, which is known as the birefringence deviates with the field-of-view angle of polarized light. The basic principle of the metrology is presented via theoretical derivation and has been verified in the static retardance measurement experiments. With a resolution test, a temporal resolution of 0.4 ms per attitude measurement and an angular resolution up to 0.0025°are achieved. With the help of a bubble level, the attitude angles of an object attached with a birefringent wave plate are obtained in the dynamic experiments, which have achieved an accuracy better than 0.02°. Additionally, the angular velocity and acceleration of the real-time measured roll angle can be extracted simultaneously. The experimental results demonstrate that the proposed metrology has great potential and advantages in the real-time attitude sensing.

https://doi.org/10.1364/OL.387626

The attitude angles are important parameters describing the motion of an object. In the fields of precision manufacturing [1], robotics control [2], and navigation of the aircraft [3], accurate and real-time monitoring of the attitude angles (yaw φ, pitch θ, and roll ϕ) is very important. Traditional attitude metrologies are based on the combination of the attitude sensor information [4], such as gyroscopes and accelerometers. Since gyroscopes suffer from integral error [5], and accelerometers are susceptible of vibration [6], the systems are usually equipped with multiple sensors in order to accurately measure the attitude angle, which makes the systems complicated and costly.

Today, due to the advantages of being noncontact, flexible, low in cost, and highly precise and sensitive, the polarimetry methods show great potential in attitude metrology. Li *et al.* [7] and Gillmer *et al.* [8] presented a compact sensor for a roll angle, which achieved a $\pm 30°$ and 43° working range, respectively. MacPherson *et al.* presented a multicore fiber incorporating fiber Bragg grating strain sensors in each core as a fiber optic pitch and roll sensor [9], which achieved the resolutions of $\pm 2°$ in roll ϕ and $\pm 15°$ in pitch θ. Saito *et al.* proposed a laser autocollimation method for measuring the attitude angle by using different diffraction light spots reflected from the diffraction gratings [10]. Although the autocollimator has a resolution of 0.01 arcsec and an accuracy of 0.5 arcsec, the measuring range is only 60 arcsec. In conclusion, the methods mentioned above have a limited measurement range and cannot achieve real-time attitude tracking. It is of great importance to develop an optical method to accurately measure the attitude angles in real time over an ultra-large measurement range.

In this Letter, we present a novel method for attitude tracking based on the high-speed polarimetry, which utilizes different phase modulations produced during the polarized light incident into the birefringent crystals along with different field-of-view angles. With the proposed method, the attitude angles can be obtained in an ultra-large measurement range, i.e., the roll angle of 0°–360°, the theoretical ranges of the yaw and pitch are $-90° - 90°$, respectively. The proposed method has been verified by the consistency achieved between the static measurements and the simulation. Additionally, in the dynamic measurement experiments, the attitude angles can be accurately measured, and the angular velocity and angular acceleration of the roll angle can be achieved simultaneously. The high precision and real-time measurement results have demonstrated the practicality and advantages of the proposed attitude metrology.

The experimental setup for the proposed attitude metrology consists of three parts: a high-speed Stokes polarimeter, a polarization state generator (PSG) and a sample stage, as described in our previous works [11]. The Stokes polarimeter with six parallel detection channels is based on the principle of spatial division of amplitude and can detect the Stokes vector of the probing light in several nanoseconds. The light source in the PSG is a 5 mW Red (632.8 nm) He–Ne Laser (THORLABS). The PSG can generate polarized light of any polarization state. The sample stage consists of a pitch adjustment stage, a yaw

adjustment stage, and a stepping motor, which can continuously change the ϕ within the range of 0–360°, and fix the φ and θ at an arbitrary value within the range of $-90° - 90°$ and $-7° - 7°$, respectively.

The birefringent device for the attitude metrology is a quartz compound zero-order wave plate, which consists of two multi-order wave plates whose optical axes are orthogonally aligned, as schematically shown in Fig. 1. In the birefringent wave plates, there are two refractive indices, i.e., the extraordinary index n_e and the ordinary index n_o, which are in the directions parallel with and perpendicular to the optical axis, respectively. It is well known that the n_e will change with the incident angle of the light incident into the crystal, while the n_o remains unchanged [12]. If the optical axis of the ith elements is parallel with the y_w-axis, the effective refractive indices along $y_w - z_w$ axis [12–14] can be expressed as

$$\begin{cases} n_{y_i} = n_{z_i}\left[1 + \left(\frac{1}{n_{z_i}^2} - \frac{1}{n_{0_i}^2}\right)\sin^2\beta\cos^2\phi\right]^{1/2} \\ n_{z_i} = n_{0_i} \end{cases}. \quad (1)$$

According to the propagation of the light in the wave plate shown in Fig. 1, the optical path difference can be written as

$$\begin{aligned} L &= n_{y_1}|\mathrm{OA}| - n_{z_1}|\mathrm{OB}| + n_{y_2}|\mathrm{AC}| - n_{z_2}|\mathrm{BD}| - |\mathrm{CD}|\sin\beta \\ &= \sum_{i=1}^{2} d_i\left(\sqrt{n_{y_i}^2 - \sin^2\beta} - \sqrt{n_{z_i}^2 - \sin^2\beta}\right), \end{aligned} \quad (2)$$

where d_i is the thickness of the ith birefringent crystal, and n_{yi} and n_{zi} are the effective refractive indices of the ith birefringent crystal along the y_w and z_w axis directions, respectively. Additionally, it should be noted that the θ and φ are coupled in the measurement of the incident angle β, where

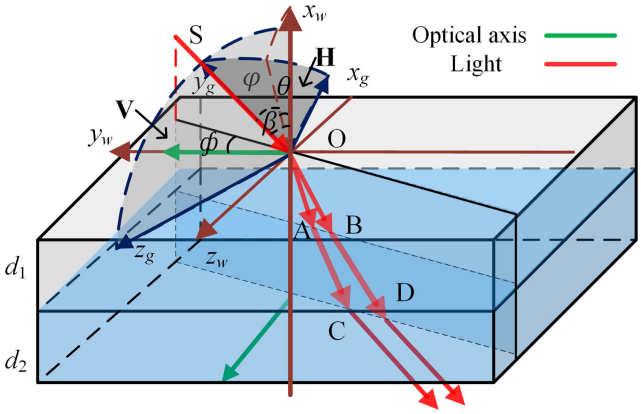

Fig. 1. Schematic of the light propagation in the composite wave plate under arbitrary attitude angles; $x_w - y_w - z_w$ is the coordinate system of the wave plate; $x_g - y_g - z_g$ is the coordinate system of the ground. **H** is the horizontal plane, which is composed of the $x_g - y_g$ axis, while **V** is the vertical plane, which is composed of the $x_w - z_g$ axis. The ϕ refers to the azimuth of the incident plane with respect to the optical axis, which also represents the roll ϕ, and β refers the incident angle of the input light. The angle between x_w axis and the projection of x_w on the **H** plane is the pitch θ, and the angle between the projection and y_g axis is the yaw φ.

$\cos\beta = \cos\theta\cos\varphi$. Then, to decouple them, the θ is measured by a bubble level, which has an accuracy of about 0.003°.

Finally, the incident light experiences a phase retardance change when traveling through the wave plate, as expressed:

$$\begin{aligned} \delta(\beta,\phi) &= \frac{2\pi}{\lambda}L = \frac{2\pi}{\lambda}\sum_{i=1}^{2} d_i\left(\sqrt{n_{y_i}^2 - \sin^2\beta}\right. \\ &\quad \left. - \sqrt{n_{z_i}^2 - \sin^2\beta}\right) \\ &= \frac{2\pi}{\lambda}d_1\left(\sqrt{n_e^2 - \frac{n_e^2\cos^2\phi + n_o^2\sin^2\phi}{n_o^2}\sin^2\beta}\right. \\ &\quad \left. - \sqrt{n_o^2 - \sin^2\beta}\right) \\ &\quad - \frac{2\pi}{\lambda}d_2\left(\sqrt{n_e^2 - \frac{n_e^2\cos^2\phi + n_o^2\sin^2\phi}{n_o^2}\sin^2\beta}\right. \\ &\quad \left. - \sqrt{n_o^2 - \sin^2\beta}\right). \end{aligned} \quad (3)$$

Inspired by the above principle, we can construct an analytical mapping between the attitude of a birefringent wave plate and its retardance. Namely, we can achieve attitude monitoring by using the field-of-view effect of birefringence. A practical birefringent device exhibits not only linear birefringence (LB), but also small linear diattenuation (LD) and circular birefringence (CB), when the light is obliquely incident [15,16]. To measure the attitude angles with polarimetry, the characterization of the wave plates in the Mueller matrix formalism can be expressed as [17]

$$\mathbf{M}_{\mathrm{wp}}(\phi,\delta,\gamma) = \mathbf{M}_{\mathrm{LB}}(\phi,\delta)\cdot\mathbf{M}_{\mathrm{CB}}(\gamma)\cdot\mathbf{M}_{\mathrm{LD}}(\phi,\psi), \quad (4)$$

where $\mathbf{M}_{\mathrm{LD}}$ and $\mathbf{M}_{\mathrm{LB}}$ are the Mueller matrix of a linear diattenuator and linear retarder, respectively, ψ and δ are the diattenuation angle and linear retardance, respectively, and ϕ is the azimuth of the fast axis. $\mathbf{M}_{\mathrm{CB}}$ is the Mueller matrix of an optical rotator with the rotation angle γ [16,17]. It should be noted that since the wave plate used is supplied with antireflection coating, the LD caused by the interface diattenuation is negligible in the retardance measurement.

In principle, the light intensity matrix **B** measured by six photomultiplier tubes can be obtained by multiplying the Stokes vector $\mathbf{S}_{\mathrm{in}}$ of the incident light, the Mueller matrix of sample **M**, and the demodulation matrix **A** of the FPMS [18]. In order to avoid the errors caused by CB and simplify the data analysis process, the δ of the wave plate is extracted from Stokes parameters S_3, when the polarization state of the incident light is left-hand circular polarization. Then the ϕ can be extracted from $S_2/\sin(\delta)$ or $S_3/\sin(\delta)$, as given by

$$\begin{aligned} \mathbf{S}_{\mathrm{out}} &= \mathbf{M}_{\mathrm{WP}}\cdot[1\ 0\ 0\ 1]^{\mathrm{T}} = \left(\mathbf{A}^{\mathrm{T}}\mathbf{A}\right)^{-1}\mathbf{A}^{\mathrm{T}}\mathbf{B} \\ &= [1\ \ \sin(2\phi)\sin(\delta)\ \ \cos(2\phi)\sin(\delta)\ \ \cos(\delta)]^{\mathrm{T}}. \end{aligned} \quad (5)$$

Based on the extracted results of δ and ϕ, we can obtain the β with Eq. (3). Since the θ is measured by a bubble level, the φ can be calculated by

$$\varphi(t) = \arccos\left[\frac{\cos\beta(t)}{\cos\theta(t)}\right]. \tag{6}$$

The proposed attitude metrology is theoretically feasible with the ϕ in the range of 0°–360°, and θ and φ in the range of $-90° - 90°$. However, limited by the clear aperture (CA) of the wave plate and the travel of the adjustment stages, we can only demonstrate our method with θ in the range of $-7°$ and 7°, and φ in the range of $-40° - 40°$ in our experiments.

The system is carefully *in situ* calibrated before performing the measurement experiments [11]. Most of the systematic errors and random noise have been compensated for in the calibration process. Then the largest error source remaining in the attitude metrology is the incident imperfect circularly polarized light. To get a circularly polarized light, we first maintain a relative angle of about 45° between the optical axis of a polarizer and that of a quarter-wave plate without samples on the polarimeter. Due to the deviation of the relative angle $\Delta\theta_{cir}$ and the deviation of the retardance $\Delta\delta_{cir}$ of the wave plate, the output light is non-ideal circularly polarized light. Then, to compensate for the deviations, the polarizer and wave plate are rotated simultaneously in the same increments. Meanwhile, the function Eq. (7) is adopted to estimate the difference between the measured and calculated Stokes vectors. By minimizing the function, we can obtain the $\Delta\theta_{cir}$ and $\Delta\delta_{cir}$ in the fitting procedure. Finally, a relatively ideal circularly polarized light can be output by compensating for the deviations:

$$\chi^2 = \sum_{q=1}^{N_m}\sum_{p=0}^{3}\left[\frac{S_{q,p}^{m} - S_{q,p}^{c}(\Delta\theta_{cir}, \Delta\delta_{cir})}{\sigma(S_{q,p})}\right]^2, \tag{7}$$

where N_m is the total number of the increment measurements, the superscripts "m" and "c" represent the measured and calculated results, respectively, the subscript "q, p" represents the pth Stokes parameter in the qth increment measurement, and $\sigma(S_{q,p})$ is the standard deviation of the measured Stokes vector.

To verify the correctness of the proposed attitude metrology, the retardance of the wave plate at different attitude angles (i.e., field-of-view angles) is measured with the Stokes polarimeter, and the results are compared with theoretical calculations. Specifically, we make one of the attitude angles vary within a certain range in the experiments, while the other two remain unchanged. It can be observed from Fig. 2 that the measured results are consistent with the simulation results, and the measured error of the retardance is less than 2°. Besides, the retardance changes versus φ and θ have the same waveform. This is because in the retardance calculation formula [Eq. (3)] the changes of φ and θ induce the same variation in the incident angle. It is impossible to distinguish them by the measured ϕ and the retardance alone, which is the reason for measuring the θ with the bubble level. Moreover, the smaller the incident angle is, the smaller is error in the retardance measurement. The relatively large error in retardance measurement at a large incident angle results from the incidence of the edge region of the wave plate limited by the effective CA of the wave plate and size of the mount. A larger measurement range can be achieved by increasing the CA of the wave plate and the size of the mount.

We also perform an angular resolution test of the ϕ with the instruments. As an example, the angular velocity of the motor

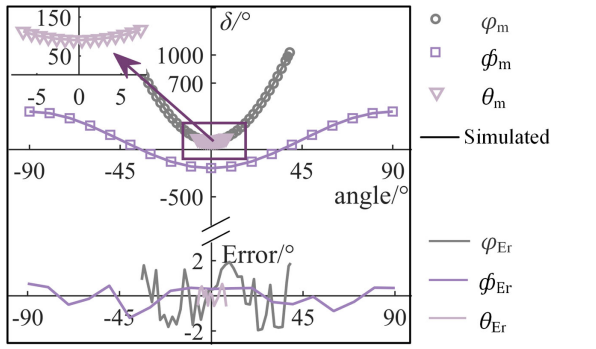

Fig. 2. Retardance of the wave plate under different attitude angles: subscripts "m" represent the measured results; subscripts "Er" represent retardance measurement errors, which are defined as simulated results minus the measurement results. (i) φ is in the range of $-34° - 39°$ when the θ is 0° and the ϕ is 100°; (ii) ϕ is in the range of $-90° - 90°$ when the θ is 0° and the φ is 20°; (iii) θ is in the range of ±7° when the φ is 0° and the ϕ is 20°.

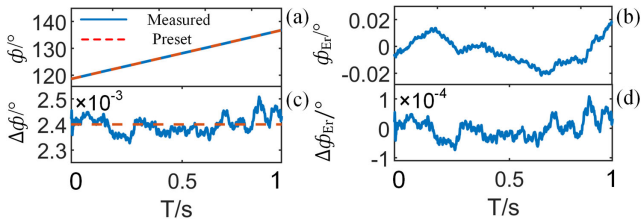

Fig. 3. Resolution test of the ϕ: "Er" represents the preset results minus the measured results. (a) Measured and preset ϕ; (b) the measurement error of ϕ; (c) the measured and preset resolution of ϕ, which is defined as $\Delta\phi(t) = \phi(t + \Delta t) - \phi(t)$, $\Delta t = 0.4$ ms; (d) the measurement error of resolution of ϕ.

is kept at 20°/s, the sampling frequency of the polarimeter is 2.5 KHz, and the measurement of the ϕ is performed with $\varphi = 0°$ and $\theta = 0°$. Additionally, the results are shown in Fig. 3. It can be observed that the measured results are consistent with the preset results. However, there is a relatively large error of about 0.02°. Since the measurement of the polarimeter is a direct measurement of the roll angel at a single time point, the error is not the cumulative error, and it is more likely due to the unstable rotation of the motor. Meanwhile, the relative errors fluctuate between ±0.02°, and the error will cancel out each other when the stepper motor runs for a long time. Besides, the measured resolution of the ϕ is better than 0.0025°, which fluctuates around the preset value 0.0024°. Additionally, the increment measurement accuracy of the ϕ is better than 0.0001°. Additionally, further improvements in motor control system will result in more accurate measurement results.

Finally, the practicality of the proposed attitude metrology is demonstrated through a varying-velocity rotation real-time measurement experiment under arbitrary attitude angles. As an example, the ϕ driven by the motor changes with time, the θ which is determined by a bubble level is fixed at 4°, and the φ is fixed at 6°. Meanwhile, the sampling frequency of the polarimeter is 2.5 KHz.

Figure 4 presents the measurement results on the ϕ changing with the time in the dynamic experiments. It can be observed that the ϕ increases with the time at different rates, as shown Fig. 4(a). In order to compare the measured results with the

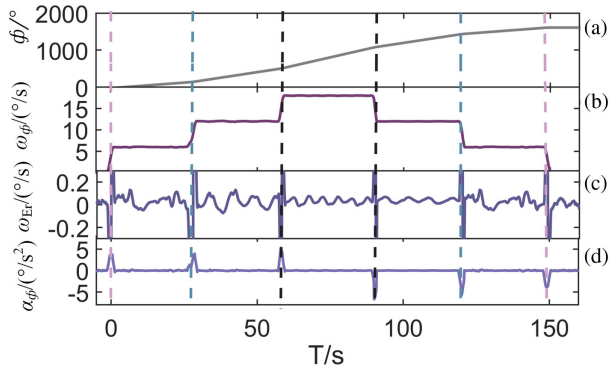

Fig. 4. Results about the ϕ in the dynamic experiments: (a) the ϕ over time, (b) ω_ϕ over time, (c) errors of ω_ϕ, and (d) α_ϕ over time.

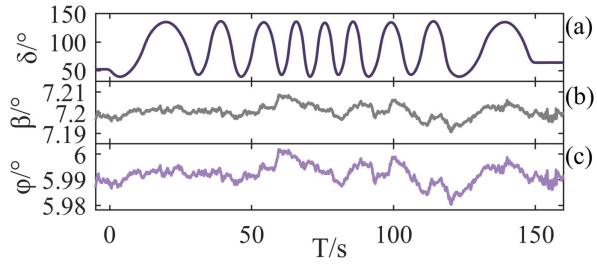

Fig. 5. (a) δ over time, (b) β over time, and (c) φ over time when the pitch angle is considered almost unchanged.

preset change process more clearly, we extract the angular velocity ω_ϕ with Eq. (8), as shown in Fig. 4(b). The measurement accuracy of the angular velocity is better than 0.1°/s over most of the time points, as shown in Fig. 4(c). Since the motor control system used can only set the angular velocity instead of the angular acceleration α_ϕ, the acceleration and deacceleration processes cannot be controlled in the preset process. This is why the measured angular velocity has relatively large errors around the acceleration and deacceleration points. Additionally, we also extract the acceleration of the ϕ with Eq. (9) to explore the uncertain acceleration and deceleration processes, as shown in Fig. 4(d). It can be seen that the absolute acceleration/deacceleration first increases and then decreases symmetrically when the velocity changes. Besides, the maximum acceleration increases with the increases of the angular velocity:

$$\omega_\phi(t) = \frac{\phi(t+\Delta t) - \phi(t)}{\Delta t}, \tag{8}$$

$$a_\phi(t) = \frac{\omega_\phi(t+\Delta t) - \omega_\phi(t)}{\Delta t}. \tag{9}$$

According to Eq. (3), we can obtain the incident angle β versus the time by the least square algorithm from the measured results of ϕ and δ, as shown in Fig. 5(a). It can be observed from Fig. 5(b) that the extracted β fluctuates around 7.20°, indicating that an irregular vibration exists in the rotation process of the wave plate. Although the bubble level cannot output the change of the θ in real time, we observed that the bubble hardly moved during the experiment time. Thus, it can be approximated that the fluctuation in the β is caused by the change of φ. Then the φ over time can be obtained by Eq. (6). It is shown in Fig. 5(c) that the φ fluctuates around 5.99° which is very close to the preset value of 6°. Additionally, in this experiment, the φ measurement accuracy is better than 0.02°. Furthermore, to get more accurate measurement results of the φ and θ, it is better to change the bubble level into a digital electronic level which can real-time output the change in θ.

In summary, a novel optical method utilizing the field-of-view effect of birefringence and a high-speed polarimetry is proposed for the noncontact real-time attitude metrology, in which a temporal resolution of 0.4 ms and an angular resolution up to 0.0025° have been achieved. We introduce the basic principle and show the correctness and efficiency of the proposed method by both the static retardance measurement and the dynamic experiments. The proposed method has been proven to be feasible with the ϕ in the range of 0°–360°. Although we can only show the measurement range $-7° - 7°$ for θ and $-40° - 40°$ for φ due to the limit of the experimental setup, their theoretical detectable ranges approach $-90° - 90°$. The results show that all the attitude angles of the object attached with a birefringent crystal can be obtained with an accuracy of 0.02°. As an additional benefit, the angular velocity and acceleration of the real-time measured roll ϕ can be extracted simultaneously, which is expected to pave the way for real-time attitude sensing.

Funding. National Natural Science Foundation of China (51975232, 51525502, 51727809, 51805193); National Key Research and Development Program of China (2017YFF0204705); Natural Science Foundation of Hubei Province (2018CFA057); National Major Science and Technology Projects of China (2017ZX02101006-004).

Disclosures. The authors declare no conflicts of interest.

REFERENCES

1. M. Xu, Y. Dai, X. Xie, and L. Zhou, Int. J. Nanomanuf. **14**, 332 (2018).
2. Y. Xu and T. Kanade, *Space Robotics: Dynamics and Control* (Springer, 1992).
3. Y. Dong, Y. Zhang, and J. Ai, Aerosp. Sci. Technol. **55**, 292 (2016).
4. J. L. Crassidis and F. L. Markley, J. Guid. Control. Dyn. **39**, 1513 (2016).
5. M. E. Pittelkau, *Encyclopedia of Aerospace Engineering*, R. Blockley and W. Shyy, eds. (Wiley, 2010).
6. R. Jin, H. Sun, J. Sun, W. Chen, and J. Chu, *IEEE Conference on Mechatronics and Automation* (IEEE, 2016), p. 2466.
7. S. Li, C. Yang, E. Zhang, and G. Jin, Opt. Lett. **30**, 242 (2005).
8. S. R. Gillmer, X. Yu, C. Wang, and J. D. Ellis, Opt. Lett. **40**, 2497 (2015).
9. W. N. MacPherson, G. M. Flockhart, R. R. Maier, J. S. Barton, J. D. Jones, D. Zhao, L. Zhang, and I. Bennion, Meas. Sci. Technol. **15**, 1642 (2004).
10. Y. Saito, Y. Arai, and W. Gao, Sens. Actuators, A **150**, 175 (2009).
11. S. Zhang, H. Gu, J. Liu, H. Jiang, X. Chen, C. Zhang, and S. Liu, J. Opt. **20**, 125606 (2018).
12. H. Gu, X. Chen, C. Zhang, H. Jiang, and S. Liu, J. Opt. **20**, 015401 (2017).
13. F. E. Veiras, L. I. Perez, and M. T. Garea, Appl. Opt. **49**, 2769 (2010).
14. H. Gu, X. Chen, H. Jiang, Y. Shi, and S. Liu, Opt. Lett. **44**, 3026 (2019).
15. H. Gu, S. Liu, X. Chen, and C. Zhang, Appl. Opt. **54**, 684 (2015).
16. O. Arteaga, A. Canillas, and G. E. Jellison, Jr., Appl. Opt. **48**, 5307 (2009).
17. H. Gu, X. Chen, Y. Shi, H. Jiang, C. Zhang, P. Gong, and S. Liu, Opt. Express. **26**, 25408 (2018).
18. A. De Martino, Y.-K. Kim, E. Garcia-Caurel, B. Laude, and B. Drévillon, Opt. Lett. **28**, 616 (2003).